Near-Infrared Room-Temperature Phosphorescence from Monocyclic Luminophores

Zi-Ang Yan, Chenjia Yin, He Tian, Xiang Ma*

Key Laboratory for Advanced Materials and Feringa Nobel Prize Scientist Joint Research Center, Frontiers Science Center for Materiobiology and Dynamic Chemistry, Institute of Fine Chemicals, School of Chemistry and Molecular Engineering, East China University of Science & Technology, No. 130 Meilong Road, Shanghai 200237, China.

ABSTRACT: Compact luminophores with long emission wavelengths have aroused considerable theoretical and practical interest. Organics with room-temperature phosphorescence (RTP) are also desirable for their longer lifetimes and larger Stokes shifts compared to fluorescence. Utilizing the low electronic transition energy intrinsic to thiocarbonyl compounds, electron-withdrawing groups were attached to the 4*H*-pyran-4-thione core to further lower the excited states energies. The resulting mini-phosphors were doped into appropriate polymer matrices. Both pure organic, amorphous materials emitted near-infrared (NIR) RTP. Having a molar mass of only 162 $g \cdot mol^{-1}$, one of the phosphors emitted RTP that peaked at 750 nm, with a very large Stokes shift of 15485 cm^{-1} (403 nm). Thanks to the good processability of the polymer film, light-emitting didoes (LEDs) with NIR emission was easily fabricated by coating doped polymer on ultraviolet LEDs. This work provides an interesting strategy to achieve NIR RTP using compact luminophores.

Photoluminescent materials with novel structures and unique properties have long been the pursuit of scientists for their theoretical values as well as broad applications.[1-8] Due to longer lifetimes and larger Stokes shifts compared to fluorescence, materials with room-temperature phosphorescence (RTP) are of particular interest and is applied to various fields.[9-16] Traditional inorganic and organo-metallic RTP typically requires harsh preparation conditions or heavy metals.[17] To avoid these drawbacks, pure organic RTP materials emerged in recent years.

For organic molecules, the transition from an excited singlet state to a triplet state is largely spin forbidden. Heavy atoms like bromine and iodine were introduced to enhance spin-orbit coupling (SOC), accelerating intersystem crossing (ISC).[18-21] Other functional groups like carbonyl can also promote ISC.[22-28] Still, triplet excitons can easily be deactivated by molecular motion and quenchers like oxygen, which make them only emissive at cryogenic temperatures and in inert atmospheres. Crystallization,[29-32] host-guest interactions,[33-35] and copolymerization[36-38] were employed to inhibit the nonradiative decay and shield the quenchers, making organic RTP possible.

Long wavelength emissions were often achieved by expansion of conjugation.[39-41] Fused ring luminophores can cause problems like limited solubility and processibility. For RTP, Stokes shifts would be reduced due to narrowed singlet-triplet energy

gap. In addition, polycyclic aromatic hydrocarbons are often carcinogenic and difficult to degrade.[42] Beyond practical concerns, the scientific question of whether small luminophores can have long wavelength emissions also became a research interest. Some researchers attached two pairs of electron donors and acceptors to a benzene ring, which is called X-shaped benzene strategy.[43-46] Used for both fluorescence and phosphorescence (Scheme 1c right), the maximum emission wavelength was 654 nm[45] and the smallest molar mass was 252 g·mol^{-1}.[43] However, no near-infrared (NIR) emission was obtained.

Herein, a different approach was taken by utilizing the low n→π* transition energy intrinsic to thiocarbonyl groups and auxiliary electron-withdrawing groups. 4*H*-pyran-4-thione (PT, Scheme 1a) was chosen as a compact core. Assisted by density functional theory (DFT) prediction, electron-withdrawing groups were designed to be attached to its *meta* positions to further lower the T_1 energies. Both of the resulting luminophores exhibited phosphorescence in solution at 77 K. Poly(methyl methacrylate) (PMMA) was then chosen as a matrix to endow them with RTP in ambient environment. Both the resulting polymer films emitted NIR RTP. Impressively, one phosphor emitted 750 nm RTP with a Stokes shift as large as 15485 cm^{-1} (λ_{abs} = 347 nm), while its molar mass is only 162 g·mol^{-1}. The amorphous character ensures that these polymer films had good processibility. Therefore, light-emitting didoes (LEDs) with NIR emission was easily fabricated by coating dye@PMMA on commercial ultraviolet (UV) LEDs. Scheme 1 illustrates this strategy and the design process.

Behaving very differently from ketones, thiones have received some attention historically,[47] but are largely neglected today. The frontier molecular orbitals of thiones involves sulfur atomic orbitals with a principal quantum number of 3. Therefore, their energies of lowest electronic transitions (n→π*) are significantly lower compared to the corresponding ketones. Other typical properties of thiones include: highly forbidden S_0→S_1 transitions; large S_2–S_1 energy gaps; and very strong SOC, resulting in ultrafast transitions between singlets and triples and direct S_0→T_1 absorbance.[47]

PT was chosen as the core because of its small size and possibility for substitution. Although PT had not been studied for ambient condition phosphorescence, its photophysical properties had been investigated at cryogenic and inert environments.[48] Basic properties were measured again using 2-MeTHF as solvent to develop a reference for the following DFT prediction of substituted molecules. As shown in Figure 1a, PT exhibited a maximum absorbance at 334 nm and a weak peak at about 519 nm. Consistent with previous findings, the former was attributed to the S_0→S_2 (π→π*) transition and the latter to the forbidden S_0→S_1 (n→π*) transition. Because of the solvent interactions herein (compared to perfluoroalkanes[48]), S_0→T_1 direct absorbance was hidden in the n→π* tail, which is slightly broadened. At 77 K, the phosphorescence of PT had two local maxima at 551 and 585 nm, which was further confirmed with delayed spectrum and decay measurement (Figure S19d, g).

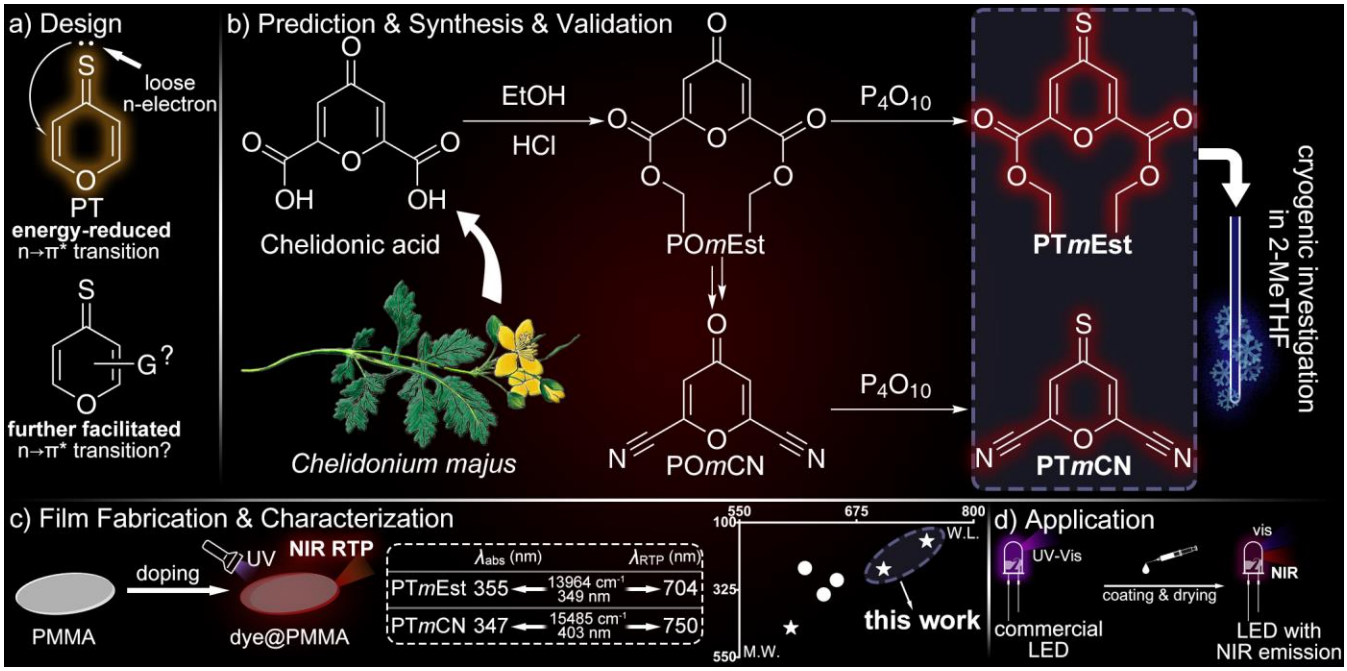

Scheme 1. Illustration of (a) initial conceptualization of mini NIR phosphors based on thiones; (b) synthesis and validation of the predicted structure; (c) film fabrication (left), characterization results (middle) and comparison with other works[43-46] (right, star: RTP; dot: fluorescence; M.W.: molecular weight; W.L.: wavelength); and (d) application as NIR-emitting LEDs.

Since the low electronic transition energy of PT was attributed to the loose n-electron localized on the sulfur atom, it is possible to further assist the excitation and lower the energy *via* substitution of an electron-withdrawing moiety on the aromatic ring. A strong conjugated electron-withdrawing functional group, cyano group, was selected. Judging from resonance theory, cyano groups should be placed on the *meta* positions relative to C=S to assist its n→π* transition, where cyano and thione groups are separated by an odd number of double bonds. Fortunately, the designed molecule (4-thioxo-4*H*-pyran-2,6-dicarbonitrile, PT*m*CN) might be reasonably synthesized (Scheme 1b). First discovered in extracts of *Chelidonium majus*, chelidonic acid offered natural *meta* substitution sites on the γ-pyrone core, which could be later thiolated. PT with ethoxycarbonyl groups as another electron-withdrawing group was synthetically possible too (diethyl 4-thioxo-4*H*-pyran-2,6-dicarboxylate, PT*m*Est) from the intermediate.

Before carrying out the syntheses, the photophysical properties of PT*m*Est and PT*m*CN were predicted. Accurate prediction of spectral maxima by DFT might be difficult, but assuming similar vibronic structures, using the calculated energy levels and experimental spectra of PT itself as a reference should be enough. Calculations were done on ORCA[49-51] at M06-2X/def2-QZVPP level. Vertical excitation energies and orbital contributions were calculated using time-dependent DFT at ground state geometries. However, because phosphorescence emission is the most interested here, triplet state geometries and vertical emission energies were calculated using unrestricted Kohn-Sham (see Supporting Information, SI).

Table 1. Calculated vertical transition energies and predicted maximum wavelengths of the dyes.

Dye	Calc. vert. energies (eV)		Pred. wavelengths (nm)	
	Excitation[a]	Emission	Absorption[a]	Emission[b]
PT (ref.)	2.42, 4.34	1.92	-	-
PT*m*Est	2.18, 4.01	1.53	578, 366	668, 719
PT*m*CN	2.08, 4.09	1.44	605, 357	702, 758
PT*o*CN	2.28, 3.97	1.66	551, 371	626, 670

Two values refer to (a) transition to S_1 and S_2, (b) two phosphorescence maxima both from T_1.

Table 1 shows that substitution on *meta* positions can cause significant redshifts for both absorption and phosphorescence. PT*m*Est and PT*m*CN could have NIR phosphorescence peaks above 700 nm, while the substitution at *ortho* positions (PT*o*CN) had limited redshift, matching the expectations. Table S1 shows that S_1 and T_1 of all calculated molecules were dominated by HOMO→LUMO transition. As all HOMOs were constructed from n orbitals on sulfur atom, only LUMOs of PT*m*Est and PT*m*CN incorporated the electron-withdrawing substitution, and the effect of *ortho*-CN on LUMO is trivial (Figures 1d–f, S20).

Based on the prediction, PT*m*Est and PT*m*CN were successfully synthesized following the planned route (see SI for details). Their solutions showed weak $S_0 \rightarrow S_1$ absorption maxima at about 602 and 627 nm, respectively, confirming that the effect of cyano groups was stronger than that of ethoxycarbonyl groups (Figure 1b, c). Interestingly, the $S_0 \rightarrow S_2$ transitions exhibited the opposite trend (Table S2), which also agreed with the calculations (Table 1). Dominated by HOMO-1→LUMO transition, the S_2 state of PT and PT*m*Est does not involve the high energy n orbital (Table S1), and the stronger electron-withdrawing substitution only shifted excitation energy towards a higher level by deepening the HOMO-1 orbital. Their $S_0 \rightarrow T_1$ absorptions were also present as a tail extending to the emission spectra discussed below.

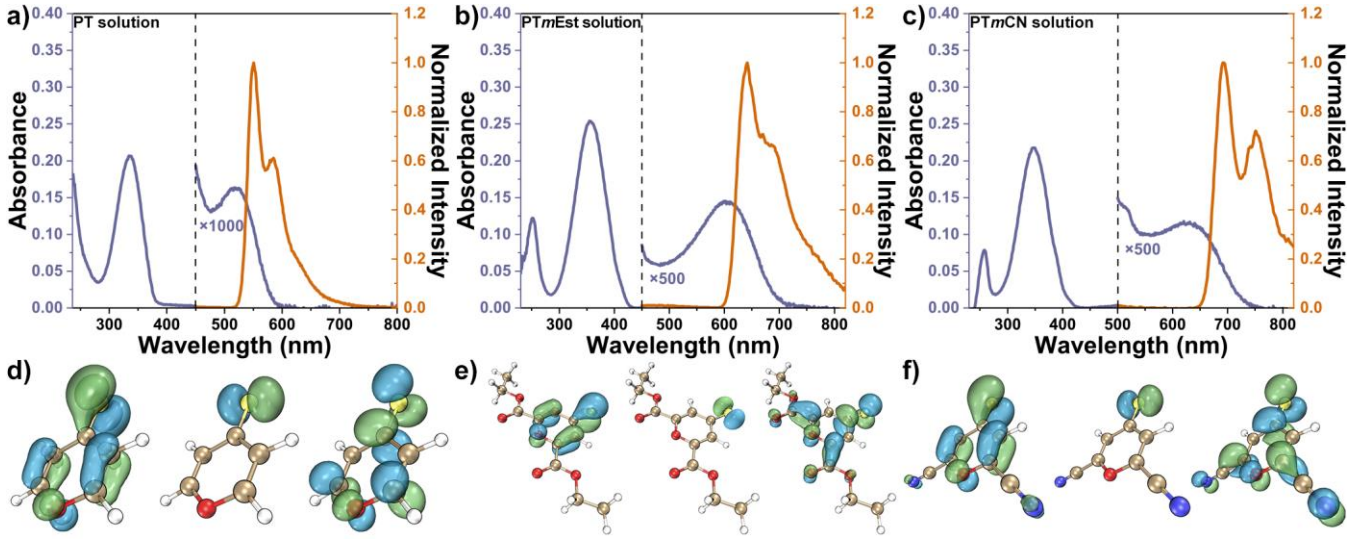

Figure 1. Absorbance (purple lines, 1×10^{-5} M) at room temperature and steady-state emission (orange lines, 1×10^{-4} M) at 77 K in 2-MeTHF solution of (a) PT, (b) PT*m*Est, and (c) PT*m*CN. HOMO-1 (left), HOMO (middle) and LUMO (right) of (d) PT, (e) PT*m*Est, and (f) PT*m*CN. Zoomed absorptions used 200 times concentrations before scaling an appropriate factor.

The solutions of the two dyes were then excited using their $S_0 \rightarrow S_2$ absorptions at 77 K (Figure 1b, c). PT*m*Est exhibited a significantly redshifted emission compared to PT, with two peaks at 641 and 691 nm. PT*m*CN redshifted even more, exhibiting emission at 696 and 753 nm. Both major and minor peaks had excitation spectra matching the absorptions and the same lifetimes (Figure S19). Rise in relative excitation intensity at $S_0 \rightarrow S_1$ absorption range was observed at higher concentrations (2×10^{-3} M), further confirming the emission species since weak absorption peaks rise more in excitation spectra, a consequence of the definition of absorbance values. The delayed spectra and decay profiles (Figure S19), along with the absence of prompt emission within 50 and 500 ns range (Figure S21) confirmed their pure delayed emission nature. Additionally, they exhibited shorter lifetimes than PT because of energy gap law. These photophysical properties were summarized in Table S2. Due to the short lifetimes and proximity between emissions and $S_0 \rightarrow S_1$ absorptions, the attribution to phosphorescence emission needed to be confirmed despite resemblance with PT. Figure S22 shows that these emission intensities decreased and decayed faster from 77 K to 137 K. At the solvent melting point, the peaks disappeared due to diffusion quenching by oxygen, confirming the phosphorescence emissions.

To endow these phosphors with NIR RTP, we set out to find a suitable polymer matrix. Ideally, polymers with hydrogen bonding networks like polyvinyl alcohol would apply. However, PMMA was chosen because thiones are sensitive to weak nucleophiles like alcohols.[52] PMMA with a high glass transition temperature would reasonably provide a rigid environment for the phosphors and shield water, *i.e.*, another nucleophile. The phosphors were respectively dissolved with PMMA in dichloromethane, followed by casting and drying (see SI). The resulting doped films were named dye@PMMA. As shown in Figure 2a and 2d, the absorptions of PT*m*Est@PMMA and PT*m*CN@PMMA were like those in solutions, including the major and forbidden peaks. NIR RTP was successfully achieved. The emissions of dyes were broadened in PMMA compared to the solutions, which was expected because of the more complex environment in polymer matrices. The delayed spectra matched the corresponding steady-state spectra and the excitation spectra also matched the absorptions, including $S_0 \rightarrow S_1$ excitation peaks due to larger concentrations (1 wt%) in films (Figure S24). Other than broadening, the relative intensities of the original two phosphorescence peaks changed in PMMA. For example, PT*m*CN solution exhibited two maxima at 696 and 753 nm at 77 K, with the former being dominant. But PT*m*CN@PMMA peaked at 750 nm. Temperature ramping experiment from 77 K (Figure 2e) shows that the emission intensity became weaker at elevating temperature, as normal phosphorescence does, but the second peak fell slower. As a result, it dominated at room temperature, further contributing to its ultralong wavelength. Calculated vibrationally resolved spectra (Figure S26c) also shows an increase in relative Franck–Condon intensity of the second peak of PT*m*CN at room temperature compared to 77 K, while the Herzberg–Teller part remained unchanged, suggesting that vibronic levels distributions were the main reason. However, geometry relaxion at higher temperatures could also contribute.

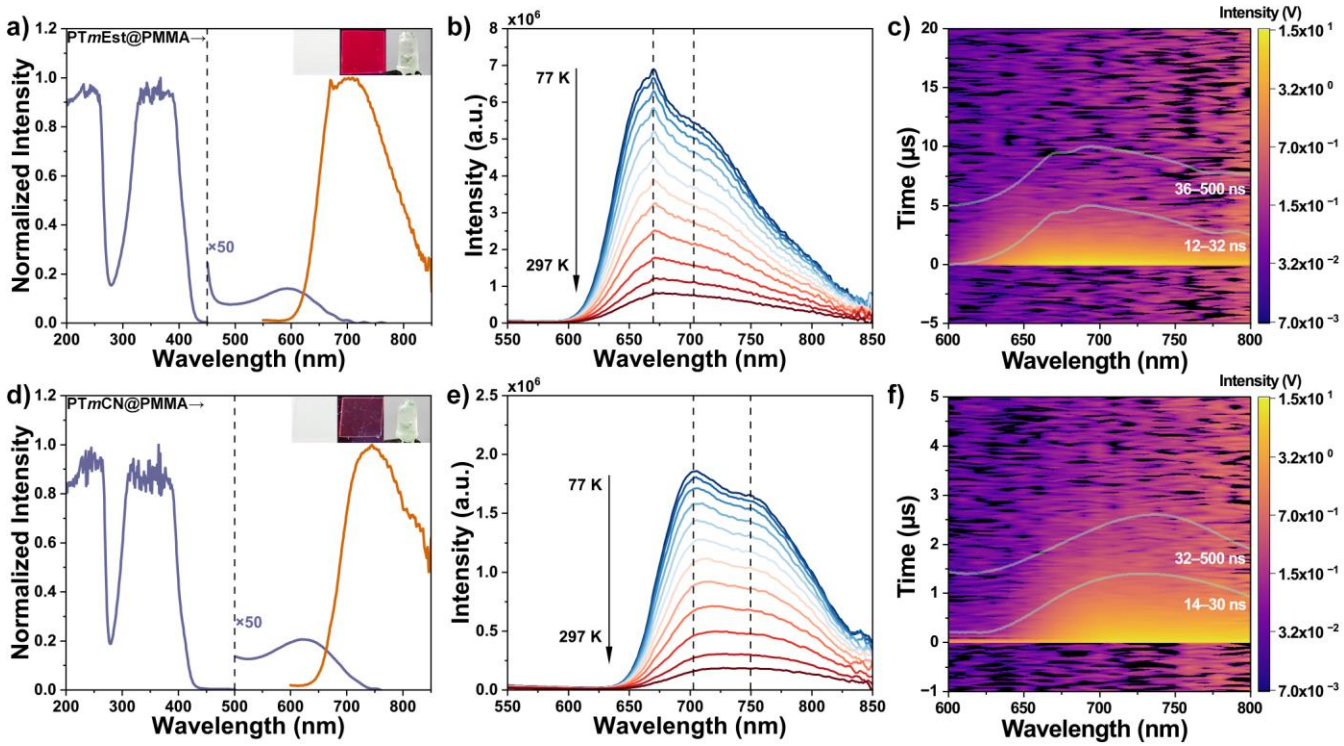

Figure 2. Spectra of (a–c) PT*m*Est@PMMA and (b–d) PT*m*CN@PMMA films in ambient environment. (a, d) Normalized absorption (purple lines) and steady-state emission (orange lines) spectra. Inset: photo of polymer films under ambient light (left) and 365 nm UV (middle), along with polymer coated LED (right). (b, e) Temperature ramping steady-state emission spectra. (c, f) Decay map and reconstructed transient spectra.

Rising temperature from 77 K caused the emission lifetimes of PT*m*Est@PMMA and PT*m*CN@PMMA to decrease (Figure S25b, c). At room temperature, due to proximity of decay curves to instrument response using microsecond flashlamp, a setup using Nd:YAG laser was used to accurately measure the emission dynamics. Decay profiles (Figure S25e, f) indicates the sub-microsecond lifetimes. Uniform decay across the wavelengths (Figure 2c, f) shows that the same peak dominated within short and long timescales, confirming the ultrafast $S_1 \rightarrow T_1$ and $T_1 \rightarrow S_0$ transitions typical of thiones, as $T_1 \rightarrow S_0$ was further accelerated according to energy gap law. The photophysical properties of dye@PMMA (including PT@PMMA) were summarized in Scheme 1c and Table S3. As shown in Figure 2 inset, the films were almost colorless under ambient light because of forbidden $S_0 \rightarrow S_1$ transitions. Under UV, red light onset could be seen from PT*m*Est@PMMA, but only dim light was observed from PT*m*CN@PMMA because most of the spectrum was outside the visible range.

Powder X-ray diffraction (Figure S27) of all doped films exhibited patterns of amorphous materials, ensuring their good processibility. Therefore, dichloromethane solutions of the phosphors and PMMA were dripped on commercial UV LEDs, followed by drying (Scheme 1d, Figure 2 inset). Energy transfer *via* trivial mechanism occurred between UV LED and dye@PMMA coatings. Electroluminescence spectra shows that LEDs with NIR emission was successfully fabricated (Figure S28), but the NIR portion was small because the visible portion of UV LEDs could not be absorbed.

In conclusion, two mini NIR phosphors with thiocarbonyl and electron-withdrawing groups were predicted and synthesized starting from a natural product. Electron deficient cores successfully facilitated the n→π* transition from the loose n-electron on sulfur, which is however very different from the donor-acceptor strategy since thiocarbonyl had not been considered as a conventional donor. NIR RTP doped films were made with a maximum RTP wavelength of 750 nm and Stokes shift of 15485 cm^{-1} (403 nm) from an emitter weighing only 162 $g \cdot mol^{-1}$. The good processibility of the polymer films allowed them to be easily coated on UV LEDs, yielding LEDs with NIR emissions. This research provides an interesting mechanism to achieve NIR RTP of small luminophores with practical values.

ASSOCIATED CONTENT

Supporting Information

The Supporting Information is available free of charge on the ACS Publications website.

Materials, methods, detailed experimental procedures, characterization of substances, and additional experimental data (PDF).

AUTHOR INFORMATION

Corresponding Author

*maxiang@ecust.edu.cn

ACKNOWLEDGMENT

We gratefully acknowledge the financial support from the National Key Research and Development Program of China (Grant No. 2022YFB3203500), the National Natural Science Foundation of China (22125803 and 22020102006), and the Fundamental Research Funds for the Central Universities.

REFERENCES

(1) Li, J.; Li, X.; Wang, G.; Wang, X.; Wu, M.; Liu, J.; Zhang, K. A direct observation of up-converted room-temperature phosphorescence in an anti-Kasha dopant-matrix system. *Nat. Commun.* **2023**, *14*, 1987.

(2) Han, P.; Zhang, G.; Wang, J.; Yao, Y.; Qiu, Y.; Xu, H.; Qin, A.; Tang, B. Z. Highly Emissive Luminogens in Both Solution and Aggregate States. *CCS Chem.* **2023**, *5*, 1686-1696.

(3) Yang, T.; Li, Y.; Zhao, Z.; Yuan, W. Z. Clustering-triggered phosphorescence of nonconventional luminophores. *Sci. China Chem.* **2023**, *66*, 367-387.

(4) Tan, J.; Li, Q.; Meng, S.; Li, Y.; Yang, J.; Ye, Y.; Tang, Z.; Qu, S.; Ren, X. Time-Dependent Phosphorescence Colors from Carbon Dots for Advanced Dynamic Information Encryption. *Adv. Mater.* **2021**, *33*, 2006781.

(5) Sedgwick, A. C.; Wu, L.; Han, H.-H.; Bull, S. D.; He, X.-P.; James, T. D.; Sessler, J. L.; Tang, B. Z.; Tian, H.; Yoon, J. Excited-state intramolecular proton-transfer (ESIPT) based fluorescence sensors and imaging agents. *Chem. Soc. Rev.* **2018**, *47*, 8842-8880.

(6) Wu, H.; Chi, W.; Baryshnikov, G.; Wu, B.; Gong, Y.; Zheng, D.; Li, X.; Zhao, Y.; Liu, X.; Ågren, H.; Zhu, L. Crystal Multi-Conformational Control Through Deformable Carbon-Sulfur Bond for Singlet-Triplet Emissive Tuning. *Angew. Chem. Int. Ed.* **2019**, *58*, 4328-4333.

(7) Wang, B.; Sun, B.; Wang, X.; Ye, C.; Ding, P.; Liang, Z.; Chen, Z.; Tao, X.; Wu, L. Efficient Triplet Sensitizers of Palladium(II) Tetraphenylporphyrins for Upconversion-Powered Photoelectrochemistry. *J. Phys. Chem. C* **2014**, *118*, 1417-1425.

(8) Liu, D.; Li, D.; Meng, H.; Wang, Y.; Wu, L. Multifunctional applications of triazine/carbazole hybrid thermally activated delayed fluorescence emitters in organic light emitting diodes. *J. Mater. Chem. C* **2019**, *7*, 12470-12481.

(9) Li, H.; Xue, X.; Cao, Y.; Cheng, H.; Luo, A.; Guo, N.; Li, H.; Xie, G.; Tao, Y.; Chen, R.; Huang, W. Achieving Stimuli-Responsive Amorphous Organic Afterglow in Single-Component Copolymer through Self-Doping. *J. Am. Chem. Soc.* **2023**, *145*, 7343-7351.

(10) Peng, H.; Xie, G.; Cao, Y.; Zhang, L.; Yan, X.; Zhang, X.; Miao, S.; Tao, Y.; Li, H.; Zheng, C.; Huang, W.; Chen, R. On-demand modulating afterglow color of water-soluble polymers through phosphorescence FRET for multicolor security printing. *Sci. Adv.* **2022**, *8*, eabk2925.

(11) Li, D.; Yang, Y.; Yang, J.; Fang, M.; Tang, B. Z.; Li, Z. Completely aqueous processable stimulus responsive organic room temperature phosphorescence materials with tunable afterglow color. *Nat. Commun.* **2022**, *13*, 347.

(12) Xie, Z.; Zhang, X.; Wang, H.; Huang, C.; Sun, H.; Dong, M.; Ji, L.; An, Z.; Yu, T.; Huang, W. Wide-range lifetime-tunable and responsive ultralong organic phosphorescent multi-host/guest system. *Nat. Commun.* **2021**, *12*, 3522.

(13) Wang, X.-F.; Xiao, H.; Chen, P.-Z.; Yang, Q.-Z.; Chen, B.; Tung, C.-H.; Chen, Y.-Z.; Wu, L.-Z. Pure Organic Room Temperature Phosphorescence from Excited Dimers in Self-Assembled Nanoparticles under Visible and Near-Infrared Irradiation in Water. *J. Am. Chem. Soc.* **2019**, *141*, 5045-5050.

(14) Liu, S.; Lin, Y.; Yan, D. Colorful ultralong room-temperature phosphorescence in dual-ligand metal-organic framework. *Chin. Chem. Lett.* **2023**, *34*, 107952.

(15) Liu, S.; Lin, Y.; Yan, D. Dynamic multi-color long-afterglow and cold-warm white light through phosphorescence resonance energy transfer in host-guest metal-organic frameworks. *Sci. China Chem.* **2023**, *66*, 3532-3538.

(16) Wang, T.; Su, X.; Zhang, X.; Nie, X.; Huang, L.; Zhang, X.; Sun, X.; Luo, Y.; Zhang, G. Aggregation-Induced Dual-Phosphorescence from Organic Molecules for Nondoped Light-Emitting Diodes. *Adv. Mater.* **2019**, *31*, 1904273.

(17) Wang, S.-F.; Su, B.-K.; Wang, X.-Q.; Wei, Y.-C.; Kuo, K.-H.; Wang, C.-H.; Liu, S.-H.; Liao, L.-S.; Hung, W.-Y.; Fu, L.-W.; Chuang, W.-T.; Qin, M.; Lu, X.; You, C.; Chi, Y.; Chou, P.-T. Polyatomic molecules with emission quantum yields >20% enable efficient organic light-emitting diodes in the NIR(II) window. *Nat. Photonics* **2022**, *16*, 843-850.

(18) Han, L.; Jin, H.; Bu, L.; Zhang, X.; Fu, X.; Qian, C.; Li, Z.; Guan, Y.; Chen, M.; Ma, Z.; Ma, Z. Altering central atoms and bromination sites of phosphorescence units to control ultralong organic room temperature phosphorescence. *Dyes Pigm.* **2024**, *227*, 112186.

(19) Dai, W.; Niu, X.; Wu, X.; Ren, Y.; Zhang, Y.; Li, G.; Su, H.; Lei, Y.; Xiao, J.; Shi, J.; Tong, B.; Cai, Z.; Dong, Y. Halogen Bonding: A New Platform for Achieving Multi-Stimuli-Responsive Persistent Phosphorescence. *Angew. Chem. Int. Ed.* **2022**, *61*, e202200236.

(20) Yang, Z.; Xu, C.; Li, W.; Mao, Z.; Ge, X.; Huang, Q.; Deng, H.; Zhao, J.; Gu, F. L.; Zhang, Y.; Chi, Z. Boosting the Quantum Efficiency of Ultralong Organic Phosphorescence up to 52 % via Intramolecular Halogen Bonding. *Angew. Chem. Int. Ed.* **2020**, *59*, 17451-17455.

(21) Yan, Z.-A.; Lin, X.; Sun, S.; Ma, X.; Tian, H. Activating Room-Temperature Phosphorescence of Organic Luminophores via External Heavy-Atom Effect and Rigidity of Ionic Polymer Matrix*. *Angew. Chem. Int. Ed.* **2021**, *60*, 19735-19739.

(22) Yao, X.; Ma, H.; Wang, X.; Wang, H.; Wang, Q.; Zou, X.; Song, Z.; Jia, W.; Li, Y.; Mao, Y.; Singh, M.; Ye, W.; Liang, J.; Zhang, Y.; Liu, Z.; He, Y.; Li, J.; Zhou, Z.; Zhao, Z.; Zhang, Y.; Niu, G.; Yin, C.; Zhang, S.; Shi, H.; Huang, W.; An, Z. Ultralong organic phosphorescence from isolated molecules with repulsive interactions for multifunctional applications. *Nat. Commun.* **2022**, *13*, 4890.

(23) Wu, H.; Baryshnikov, G. V.; Kuklin, A.; Minaev, B. F.; Wu, B.; Gu, L.; Zhu, L.; Ågren, H.; Zhao, Y. Multidimensional Structure Conformation of Persulfurated Benzene for Highly Efficient Phosphorescence. *ACS Appl. Mater. Interfaces* **2021**, *13*, 1314-1322.

(24) Wu, B.; Wu, H.; Gong, Y.; Li, A.; Jia, X.; Zhu, L. A chiral single-component sol–gel platform with highly integrated optical properties. *J. Mater. Chem. C* **2021**, *9*, 4275-4280.

(25) Guo, D.; Wang, Y.; Chen, J.; Cao, Y.; Miao, Y.; Huang, H.; Chi, Z.; Yang, Z. Intrinsic persistent room temperature phosphorescence derived from 1*H*-benzo[*f*]indole itself as a guest. *Chin. Chem. Lett.* **2023**, *34*, 107882.

(26) Wang, T.; Wang, X.; Yan, Q.; Zhang, K. Ultralong organic room-temperature phosphorescence modulated by balancing intramolecular charge transfer and localized excitation character of excited states. *Dyes Pigm.* **2024**, *224*, 112024.

(27) Pham, T. C.; Cho, M.; Nguyen, V.-N.; Nguyen, T. K. V.; Kim, G.; Min, S.; Kim, M.-R.; Yoon, J.; Lee, S. Regulating $^1O_2$ generation from heavy-atom-free triplet photosensitizers based on thiophene-fused BODIPY. *Dyes Pigm.* **2023**, *219*, 111617.

(28) He, Z.; Gao, H.; Zhang, S.; Zheng, S.; Wang, Y.; Zhao, Z.; Ding, D.; Yang, B.; Zhang, Y.; Yuan, W. Z. Achieving Persistent, Efficient, and Robust Room-Temperature Phosphorescence from Pure Organics for Versatile Applications. *Adv. Mater.* **2019**, *31*, 1807222.

(29) Singh, M.; Liu, K.; Qu, S.; Ma, H.; Shi, H.; An, Z.; Huang, W. Recent Advances of Cocrystals with Room Temperature Phosphorescence. *Adv. Opt. Mater.* **2021**, *9*, 2002197.

(30) Wang, T.; Hu, Z.; Nie, X.; Huang, L.; Hui, M.; Sun, X.; Zhang, G. Thermochromic aggregation-induced dual phosphorescence via temperature-dependent sp^3-linked donor-acceptor electronic coupling. *Nat. Commun.* **2021**, *12*, 1364-1372.

(31) Tu, L.; Fan, Y.; Bi, C.; Xiao, L.; Li, Y.; Li, A.; Che, W.; Xie, Y.; Zhang, Y.; Xu, S.; Xu, W.; Li, Q.; Li, Z. How temperature and hydrostatic pressure impact organic room temperature phosphorescence from H-aggregation of planar triarylboranes and the application in bioimaging. *Sci. China Chem.* **2023**, *66*, 816-825.

(32) Huang, L.; Chen, B.; Zhang, X.; Trindle, C. O.; Liao, F.; Wang, Y.; Miao, H.; Luo, Y.; Zhang, G. Proton-Activated "Off–On" Room-Temperature Phosphorescence from Purely Organic Thioethers. *Angew. Chem. Int. Ed.* **2018**, *57*, 16046-16050.

(33) Yin, C.; Yan, Z.-A.; Yan, R.; Xu, C.; Ding, B.; Ji, Y.; Ma, X. A 3D Phosphorescent Supramolecular Organic Framework in Aqueous Solution. *Adv. Funct. Mater.* **2024**, *34*, 2316008.

(34) Nie, H.; Wei, Z.; Ni, X.-L.; Liu, Y. Assembly and Applications of Macrocyclic-Confinement-Derived Supramolecular Organic Luminescent Emissions from Cucurbiturils. *Chem. Rev.* **2022**, *122*, 9032-9077.

(35) Ma, X.-K.; Liu, Y. Supramolecular Purely Organic Room-Temperature Phosphorescence. *Acc. Chem. Res.* **2021**, *54*, 3403-3414.

(36) Dou, X.; Wang, X.; Xie, X.; Zhang, J.; Li, Y.; Tang, B. Advances in Polymer-Based Organic Room-Temperature Phosphorescence Materials. *Adv. Funct. Mater.* **2024**, *34*, 2314069.

(37) Xu, Q.; Ma, L.; Lin, X.; Wang, Q.; Ma, X. Influence of the alkyl side chain length on the room-temperature phosphorescence of organic copolymers. *Chin. Chem. Lett.* **2022**, *33*, 2965-2968.

(38) Chen, H.; Yao, X.; Ma, X.; Tian, H. Amorphous, Efficient, Room-Temperature Phosphorescent Metal-Free Polymers and Their Applications as Encryption Ink. *Adv. Opt. Mater.* **2016**, *4*, 1397-1941.

(39) Hayakawa, M.; Tang, X.; Ueda, Y.; Eguchi, H.; Kondo, M.; Oda, S.; Fan, X.-C.; Iswara Lestanto, G. N.; Adachi, C.; Hatakeyama, T. "Core–Shell" Wave Function Modulation in Organic Narrowband Emitters. *J. Am. Chem. Soc.* **2024**, *146*, 18331-18340.

(40) Wu, H.; Lee, S.; Kim, H.; Hong, S.; Kim, T.; Yeo, S.; Lee, W. K.; Yoon, I. Long-wavelength absorbing and mitochondria or lysosome organelle-targeting photosensitizers with flexible or rigid terminus for fluorescence imaging and high-performance photodynamic therapy. *Dyes Pigm.* **2024**, *224*, 112039.

(41) Zong, Z.; Zhang, Q.; Qu, D.-H. A Single-Fluorophore Multicolor Molecular Sensor That Visually Identifies Organic Anions Including Phosphates. *CCS Chem.* **2024**, *6*, 774-782.

(42) Thacharodi, A.; Hassan, S.; Singh, T.; Mandal, R.; Chinnadurai, J.; Khan, H. A.; Hussain, M. A.; Brindhadevi, K.; Pugazhendhi, A. Bioremediation of polycyclic aromatic hydrocarbons: An updated microbiological review. *Chemosphere* **2023**, *328*, 138498.

(43) Tang, B.; Wang, C.; Wang, Y.; Zhang, H. Efficient Red-Emissive Organic Crystals with Amplified Spontaneous Emissions Based on a Single Benzene Framework. *Angew. Chem. Int. Ed.* **2017**, *56*, 12543-12547.

(44) Liu, B.; Di, Q.; Liu, W.; Wang, C.; Wang, Y.; Zhang, H. Red-Emissive Organic Crystals of a Single-Benzene Molecule: Elastically Bendable and Flexible Optical Waveguide. *J. Phys. Chem. Lett.* **2019**, *10*, 1437-1442.

(45) Xiang, Z.; Wang, Z.-Y.; Ren, T.-B.; Xu, W.; Liu, Y.-P.; Zhang, X.-X.; Wu, P.; Yuan, L.; Zhang, X.-B. A general strategy for development of a single benzene fluorophore with full-color-tunable, environmentally insensitive, and two-photon solid-state emission. *Chem. Commun.* **2019**, *55*, 11462-11465.

(46) Wu, Y.; Gui, H.; Ma, L.; Zou, L.; Ma, X. Red-light emissive phosphorescent polymers based on X-shaped single benzene. *Dyes Pigm.* **2022**, *198*, 110005.

(47) Maciejewski, A.; Steer, R. P. The Photophysics, Physical Photochemistry, and Related Spectroscopy of Thiocarbonyls. *Chem. Rev.* **1993**, *93*, 67-98.

(48) Steer, R. P.; Ramamurthy, V. Photophysics and Intramolecular Photochemistry of Thiones in Solution. *Acc. Chem. Res.* **1988**, *21*, 380-386.

(49) Neese, F. The ORCA program system. *Wiley Interdiscip. Rev.: Comput. Mol. Sci.* **2012**, *2*, 73-78.

(50) Neese, F. Software update: the ORCA program system, version 4.0. *Wiley Interdiscip. Rev.: Comput. Mol. Sci.* **2017**, *8*, e1327.

(51) Neese, F.; Wennmohs, F.; Beeker, U.; Riplinger, C. The ORCA quantum chemistry program package. *J. Chem. Phys.* **2020**, *152*, 224108.

(52) Ozturk, T.; Ertas, E.; Mert, O. A Berzelius Reagent, Phosphorus Decasulfide (P_4S_{10}), in Organic Syntheses. *Chem. Rev.* **2010**, *110*, 3419-3478.

263

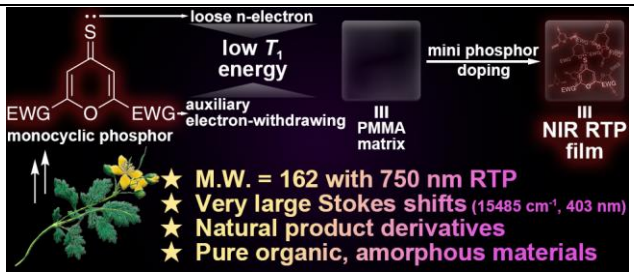

264